

# Performance evaluation of mail-scanning cameras

**Umesh Rajashekar**\*

The University of Texas at Austin  
Department of Electrical and Computer Engineering  
Laboratory for Image and Video Engineering  
1 University Station C0803  
Austin, Texas 78712-0240

**Tony Tuan Vu**

**John E. Hooning**

Autim, Inc.  
4001 Kennett Pike  
Suite 134-245  
Greenville, Delaware 19807

**Alan Conrad Bovik**

The University of Texas at Austin  
Department of Electrical and Computer Engineering  
Laboratory for Image and Video Engineering  
1 University Station C0803  
Austin, Texas 78712-0240

---

**Abstract.** Letter-scanning cameras (LSCs) form the front-end imaging systems for virtually all mail-scanning systems that are currently used to automatically sort mail products. As with any vision-dependent technology, the quality of the images generated by the camera is fundamental to the overall performance of the system. We present novel techniques for objective evaluation of LSCs using comparative imaging—a technique that involves measuring the fidelity of target images produced by a camera with reference to an image of the same target captured at very high quality. Such a framework provides a unique opportunity to directly quantify the camera's ability to capture real-world targets, such as handwritten and printed text. Noncomparative techniques were also used to measure properties such as the camera's modulation transfer function, dynamic range, and signal-to-noise ratio. To simulate real-world imaging conditions, application-specific test samples were designed using actual mail product materials. © 2010 SPIE and IS&T. [DOI: 10.1117/1.3421975]

---

## 1 Introduction

Advances in computing and vision processing technology, in particular, optical character recognition software, have made the practical implementation of automatic mail-sorting systems possible. As with any vision-dependent technology, the fidelity of the images acquired by the camera(s) is fundamental to the overall performance of these

complex systems. A method for quantifying the performance of the front-end cameras can also be used as a maintenance tool for measuring performance drift and assisting in defining the source of system change. In the event of having to upgrade the front-end camera, such an objective image fidelity assessment algorithm can be used to compare and contrast cameras from competing camera vendors. This paper outlines methods for quantifying the performance of scanning cameras used to acquire the digital images of mail products processed in sorting systems. In covering this subject, the focus will be on letter-scanning camera (LSC) systems. However, the proposed technology will have equal relevance and application for other imaging devices.

It is standard practice to measure the objective quality of imaging devices by taking images of carefully designed standardized test patterns, such as sinusoidal patterns and edges.<sup>1,2</sup> The resulting images are then analyzed using image-processing algorithms to measure camera parameters such as the modulation transfer function (resolution), dynamic range, distortion, camera noise, etc. In this paper, we group such techniques under the title of objective quantitative measurement analysis (OQMA). The use of sinusoidal and edge patterns are based on strong assumptions on the linearity of the overall imaging system.<sup>3</sup> Owing to several sources of nonlinearity during the image-acquisition process, OQMA measurements do not always generalize to real-world targets, such as images or handwritten text. To address this issue, we introduce a novel approach for objective qualitative analysis of imaging systems through comparative imaging, in which we measure the fidelity of an image produced by the LSC with reference to a high-

---

\* Address all correspondence to: Umesh Rajashekar, 4 Washington Place, Room 809, New York, New York 10003; E-mail: umesh.rajashekar@gmail.com

Paper 09209R received Nov. 3, 2009; revised manuscript received Mar. 10, 2010; accepted for publication Mar. 23, 2010; published online May 11, 2010.

quality version of the target image. Toward this end, we introduce a recent and very powerful image-quality algorithm known as the structural similarity (SSIM) index<sup>4,5</sup> to provide this measure of image fidelity. We also present modifications to SSIM that makes the measurements invariant to illumination changes. We group such comparative techniques under the broad umbrella of objective qualitative comparative analysis (OQCA).

Both OQMA and OQCA methodologies require targets with calibrated patterns that can be scanned by the LSC. Most commercial test patterns are expensive because they are designed to exacting standards for evaluating high-end imaging devices. We discovered that such commercial test patterns were superfluous for the low-resolution LSCs. The test samples used for our application were manufactured in high volume and at relatively low cost by using high-performance laser and ink-jet printers. This also gave us an opportunity to simulate a vast array of real-world mail conditions by printing the patterns on actual mail product materials.

The rest of the paper is organized as follows. We begin with a brief overview of the LSC system in Section 2, with emphasis on various distortions that can be introduced during the imaging process. The design of test patterns for measuring imaging quality in mail scanning systems is then discussed in Section 3. We introduce the SSIM image-quality index and its variations for various OQCA measurements for our application in Section 4. This is followed by a brief discussion of several OQMA techniques in Section 5. The paper concludes with discussions in Section 6.

## 2 The LSC

The LSC is a key component of the mail-sorting system responsible for acquiring digital images of the mail products as they rapidly move by the device. The function of the LSC is to scan the entire letter face and produce an 8-bit gray-scale digital image with sufficient quality in order that the address information may be recognized and read by optical character recognition (OCR) software. The LSC is an integrated subsystem comprised of the following four elements:

1. **Linear array sensors:** These are solid state devices (CCD or CMOS) that produce electrons when exposed to light photons. The sensor electronics are responsible for reading out the produced electrons and digitizing the analog signal. The readout of the linear array is accurately synchronized with the speed of the letter product as it goes by the stationary sensor. The accuracy for which the sensor readout is matched to the letter speed determines horizontal resolution. The linear array and its associated electronics influence the following baseline LSC specifications: resolution (horizontal and vertical), light sensitivity, dynamic range, and signal-to-noise ratio (SNR).
2. **Optics:** The optical component used in a LSC is designed to operate at very close working distances on the order of a few inches. Large-format lenses with low distortion, excellent light throughput, and good resolving power [measured via modulation transfer functions<sup>3</sup> (MTFs)] are typically utilized. Filters are commonly used to improve performance by optimiz-

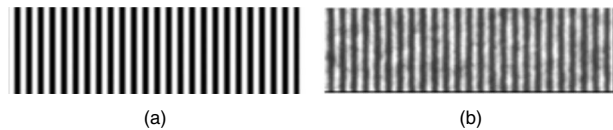


**Fig. 1** Testing the quality of resolution patterns printed using a 600-dpi laser printer: (a) an image of a 150-line/in. pattern generated digitally and (b) the result of printing this pattern using a 600-dpi laser printer and then imaging the image using a high-resolution digital camera. The printed image has a lower quality, but sufficient contrast to resolve a line pattern of 150 lines/in.

ing the visible spectrum and cutting near-IR wavelengths. The camera parameters influenced by the optics include effective resolution, light throughput, depth-of-field, evenness of vertical illumination, and optical distortion.

3. **Lighting:** The lighting component is typically a high-intensity line illumination projected on the letter at the same subject plane location as the linear array. The diffuse nature and reflective interaction of light with the letter has significant effect on defining image quality for the many types of materials letter products are made from. Evenness of illumination and flare are also affected by the lighting design, light line width, and alignment of the illumination with the linear sensor.
4. **Transport interface:** The transport interface is a mechanical component that is responsible for presenting the letter to the camera in the best possible condition and orientation. Ideally, it flattens the letter, removes folds, and prevents gaps between plastic address windows and the letter inserts. This mechanical interface can introduce geometric distortions such as skew and motion blur, which in turn affect LSC resolution and acquisition consistency.

## 3 Design of Stimuli for LSCs

It is standard practice to use calibrated test charts to evaluate performance and measure compliance for a broad range of imaging input and output devices, including digital cameras, scanners, optics, displays, and printers.<sup>2</sup> A wide variety of application-specific test charts and targets have been developed by standards organizations (ISO, NIST, and ANSI) and technology corporations (such as Eastman Kodak). Commercial test targets and charts are expected to function with extremely high-resolution analog and digital imaging systems and therefore must be made to repeatable, exact standards. The exact production tolerances typically require the use of photographic processes and special materials. The pricing ranges from \$10 to over \$200 per copy.

For our application, the quality of the imaging mechanism was not high enough to warrant these precision target templates. Current generation LSCs produce a theoretical maximum scanning resolution of 256 dpi. Thus, the test patterns used must be produced to a repeatable accuracy of at least this amount. To keep the costs of printing low, we decided to investigate the option of printing test pieces using commercial printers. The images in Fig. 1 show a computer-generated 150-lines-per-inch image and a printed (using a 600-dpi laser printer) result as viewed with a

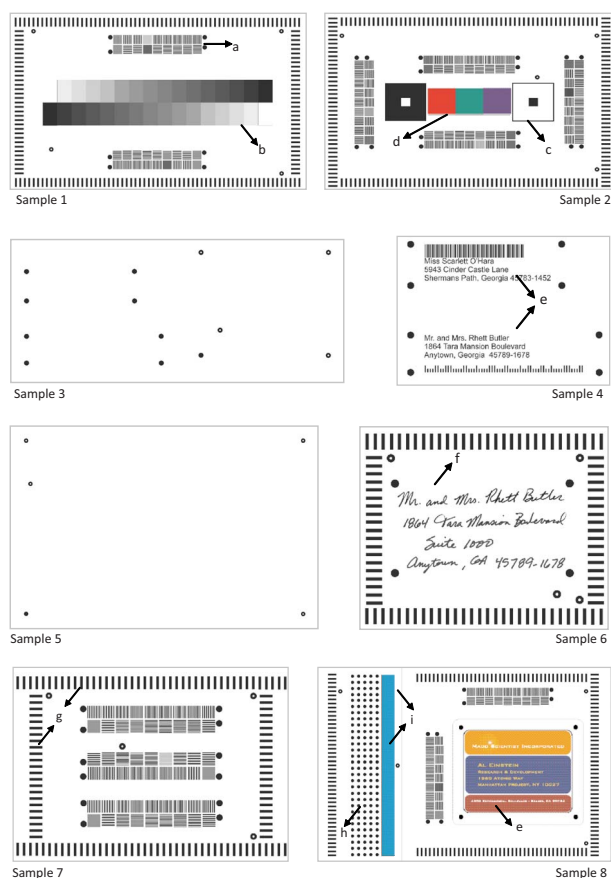


**Fig. 2** Examples of test patterns used for OQMA and OQCA measurements of LSCs. Specific patterns, indicated by the labels, correspond to a particular camera distortion as described by Table 2.

high-resolution camera (with a sampling of  $\sim 2000$  pixels per inch). Despite the slightly lower quality of the printed image, the line pairs have sufficient contrast and can be resolved without much difficulty. As the upper limit of the LSC resolution is 256 dpi, this suggests that test patterns generated by a 600-dpi laser printer have sufficient contrast to resolve 150 line pairs per inch (or a dot resolution of 300 dpi). It is relevant to mention that unlike older printers that use halftone patterns to generate gray scales, recent models of photoquality inkjet printers are optimized for producing continuous-tone gray-scale patterns. In addition to keeping the cost of printing targets low, the option of using commercial printers gave us the opportunity of generating application-specific targets, which would not be possible with standardized targets. In particular, the LSC needs to accommodate letter envelopes, cards, and folded sheets made from and printed with various combinations of paper material and ink. Address information must be resolved through plastic envelope windows. Addresses can be handwritten or typed in any font with no limitation as to the colors used. With this in mind, we created several targets that include different types of paper and envelopes with transparent windows as shown in Fig. 2 and described in Table 1. As indicated in Table 2, each test image in Fig. 2 has specific patterns (indicated by alphabetical labels) that are used to probe a particular parameter of the imaging

**Table 1** Description of the test samples used for OQCA/OQMA measurements. All patterns printed using an HP laser printer unless noted otherwise.

Sample no.	Details
1	8.5×5.5 in. folded card. Gray-scale pattern was printed on HP ink-jet printer and HP photopaper
2	8.5×5.5 in. folded card
3A/3B	8.875×3.875 in. standard double window envelope stuffed with white papers to simulate thin (3A) and thick (3B) envelopes
4A/4B	8.875×3.875 in. standard double window envelope stuffed with printed address on white papers to simulate thin (4A) and thick (4B) envelopes
5	6×9 in. clasp envelope
6	5.75×4.375 in. envelope
7	5.5×4.25 in. post card
8A/8B	6×9 in. clasp envelope stuffed with papers to simulate thin (8A) and thick (8B) envelopes

system using OQMA and/or OQCA. The specific methodology of how these patterns were used to measure imaging quality is described in Sections 4 and 5.

#### 4 OQCA

As mentioned in Section 1, imaging quality cannot solely be determined based on measurements of dynamic range, signal-to-noise ratio, and effective resolution. A better way to evaluate the performance of an image digitization/input device is to scan application-specific targets and directly measure the fidelity of the acquired images with reference to the original target. We call this process of comparing an acquired image to the original image objective qualitative comparative analysis (OQCA). OQCA is a topic that has been studied for nearly 50 years. Common measures such as the mean-squared-error (MSE) and peak SNR have, in extensive studies, been shown to provide poor correlation with human subjective evaluation of image quality.<sup>6,7</sup> By extension, these measures do not perform well at predicting how well machine vision systems will perform on distorted images. We propose to apply one of the recent and successful OQCA algorithms, known as the SSIM Index,<sup>4,5</sup> to the evaluation of mail-scanning cameras. SSIM has the advantages of extreme conceptual and computational simplicity coupled with performance better than essentially all existing algorithms, as measured in large human studies using the LIVE image database.<sup>8</sup> Although it is true that human judgments may be less important for applications such as OCR, SSIM is a natural, general image fidelity metric with broad relevance.<sup>9-12</sup>

**Table 2** Description of specific patterns in the test images and the corresponding parameter they were designed to measure.

Pattern label	Measurement	OQMA	OQCA
<i>a</i>	Horizontal and vertical resolution (line pairs per inch)	Yes	Yes
<i>b</i>	Dynamic range and SNR	Yes	No
<i>c</i>	Optical flare	Yes	No
<i>d</i>	RGB spectral reflectance and range	Yes	No
<i>e</i>	Printed text fidelity	No	Yes
<i>f</i>	Handwritten text fidelity	No	Yes
<i>g</i>	Horizontal/vertical skew	Yes	No
<i>h</i>	Pin-cushion distortion	Yes	No
<i>i</i>	Light evenness	Yes	Yes

The SSIM index between two images,  $I$  and  $J$ , is defined as the product of the local measurements of similarity of luminance, contrast, and structure as follows:

$$SSIM_{I,J} = \underbrace{\left( \frac{2\mu_I\mu_J + C_1}{\mu_I^2 + \mu_J^2 + C_1} \right)}_{\text{luminance similarity}} \underbrace{\left( \frac{2\sigma_I\sigma_J + C_2}{\sigma_I^2 + \sigma_J^2 + C_2} \right)}_{\text{contrast similarity}} \underbrace{\left( \frac{2\sigma_{IJ} + C_2}{2\sigma_I\sigma_J + C_2} \right)}_{\text{structure similarity}}, \quad (1)$$

where  $\mu_I, \mu_J$  are the weighted luminance (mean) of image  $I$  and  $J$ , respectively;  $\sigma_I, \sigma_J$  are the weighted contrasts (standard deviation) of image  $I$  and  $J$ , respectively;  $\sigma_{IJ}$  is the weighted cross correlation between  $I$  and  $J$ ; and  $C_i$  is the stabilizing constant.

In practice, the SSIM index is computed locally within a moving window across the image, resulting in a map of local SSIM values, or SSIM map. Thus, each pixel is given a SSIM value reflecting the quality of the image immediately surrounding the pixel. The SSIM map is then averaged across the image, resulting in a single SSIM index value describing the quality/fidelity of the overall distorted image with respect to the reference image. A value of 1.0

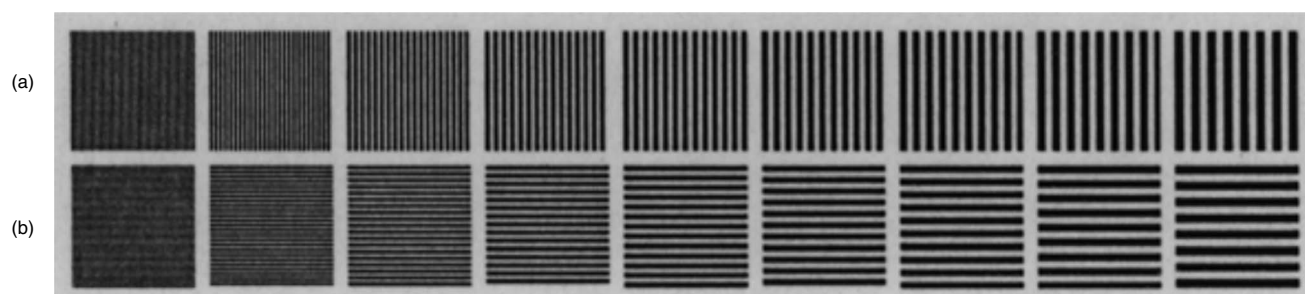
indicates a perfect match. Details of the metric and its advantages over the MSE can be found in Ref. 4. We used an  $11 \times 11$  Gaussian (standard deviation=1.5 pixels) as the weighting/windowing function and set  $C_1=(0.01 \times 255)^2$  and  $C_2=(0.03 \times 255)^2$ . The performance of SSIM has been found to be fairly insensitive to slight variations of these parameters.<sup>4</sup>

The rest of this section describes how we used the SSIM index to quantify some of the LSC parameters. For all OQCA measurements, we used a high-resolution scan (obtained via a 600-dpi flatbed scanner) of the printed test samples as the reference image against which the scans of the LSC were compared. The distortions introduced by the scanner, if any, were negligible in comparison to the ones introduced by the mail scanning cameras.

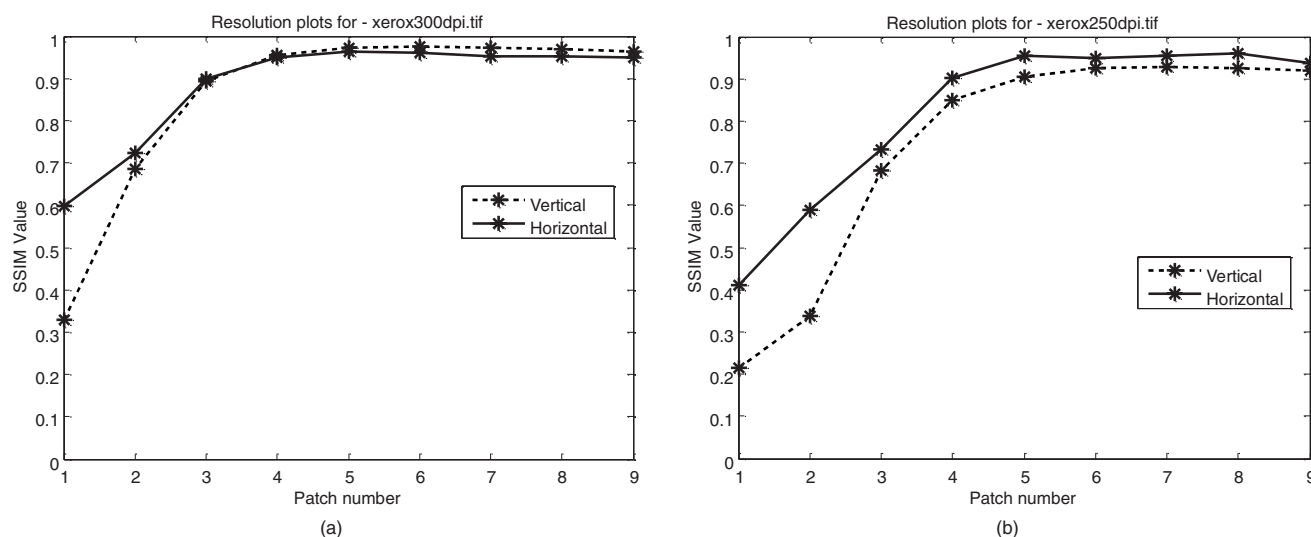
#### 4.1 Effective Resolution

Image sharpness or resolution is arguably the most important feature of an imaging device. Resolution is usually measured based on the ability of a human or a computer algorithm to resolve images of line pairs produced by the system. As seen from Fig. 2, several of the test targets contain line pairs of increasing spatial frequencies (pattern *a*) for measuring effective spatial resolution of the LSC. The larger the number of line pairs per inch that are resolved, the better the effective resolution is. It is a known fact that owing to the low-pass nature of most optical systems, the fidelity of the line pairs imaged by an optical system decreases with increasing line density. Figure 3 shows an image of one such printed resolution pattern scanned at 600 dpi, and used as the “reference” image for the SSIM-based resolution measurements. The SSIM index between this high-quality 600-dpi image and the scans produced by the LSC was computed for each of the patches and used to measure the effective resolution of the camera. As proof of principle, we use the images produced by a 350- and 250-dpi scanners (in lieu of images produced by the LSC) and measured the loss in fidelity. The SSIM index for each of these line pair spacings are shown in Fig. 4. As expected, for both scans, the quality of reproduction is high at the low spatial frequency (i.e., patch 9), and falls for high spatial frequencies (patch 1).

This resolution measurement, however, is influenced by the ambient illumination. Figure 5(a) shows a simulation of a cosinelike ambient illumination superimposed on the scan



**Fig. 3** A 600-dpi scan of line pair images used to measure the resolution of LSCs using the SSIM index: (a) used to measure the effective vertical resolution and (b) used to measure the effective horizontal spatial resolution. The number of lines pairs per inch in each patch starting from the left are 150, 100, 75, 60, 50, 43, 37.5, 33.3, and 30.



**Fig. 4** OQCA measurements of resolution for (a) a 300-dpi scanner and (b) a 250-dpi scanner. The reference image was a 600-dpi scanned image. Each plot shows the SSIM value as a function of the patch number for the image in Fig. 3. As seen at lower patch numbers (higher spatial frequency), the quality of the 250-dpi scanner is lower than the 300 dpi. The two curves within each panel correspond to the horizontal and vertical bars in Fig. 3.

from the 300-dpi scanner. As seen in Fig. 5(b), the SSIM index (and, hence, the effective resolution) is modulated by the ambient illumination. Unfortunately, ignoring just the luminance term of the SSIM Index is insufficient to handle illumination changes because the contrast term is still sensitive to mean luminance. We account for this by modifying the definition of the SSIM Index as follows:

$$\text{SSIM}_{I,J} = \left( \frac{2\mu_I\mu_J + C_1}{\mu_I^2 + \mu_J^2 + C_1} \right) \left[ \frac{2\frac{\sigma_I\sigma_J}{\mu_I\mu_J} + C_2}{(\sigma_I/\mu_I)^2 + (\sigma_J/\mu_J)^2 + C_2} \right] \times \left( \frac{2\sigma_{IJ} + C_3}{\sigma_I\sigma_J + C_3} \right). \quad (2)$$

Using this modified definition of SSIM, we can now compute the resolution values using only the contrast and the structure terms. As seen in Fig. 5(c), the modified SSIM is invariant illumination changes and the resulting graph is identical to Fig. 4(a). In the event of having to choose between LSCs from different vendors, the user can also determine a particular fixed patch number of acceptable quality (e.g., patch 3), and pick the camera that produces the highest SSIM index. For example, on examining the SSIM index value at patch 3 in Fig. 4, we see that the SSIM value is much higher for the 300-dpi scan than it is for the 250-dpi scan.

#### 4.2 Handwritten/Typed Text

Although the measurement of resolution provides a good indication of the quality of the imaging device, it does not provide a direct indication of the quality of handwritten text—one of the main targets of the LSC. There is no existing metric for evaluating the quality of printed or handwritten text. However, in our approach, where we have access to both the high-quality image of the target and scanned image of the target, the SSIM index can be used to

measure the quality of text as follows. As before, we used the 600-dpi high-resolution scan of a handwritten document [Fig. 6(a)] as our reference image (also see pattern *f* in Fig. 2). The image produced by a LSC, which has a lower quality, is shown in Fig. 6(b). Figure 6(c) shows the SSIM index map between these two images. Bright regions in the SSIM index map correspond to good image fidelity, while dark regions correspond to poor image fidelity. The SSIM index between these images turns out to be rather high (around 0.813) because the background does not have severe structural distortions. Because we were interested only in the quality of the text, we used the reference image to create a binary mask that highlighted only the text area and computed the mean SSIM value only within this map as shown in Fig. 6(d). As expected, the SSIM index of the handwritten text is lower ( $\sim 0.5$ ) reflecting the blurred text quality in image produced by the LSC. In addition to handwritten text, we also used typed-text labels as shown in Fig. 2 (pattern *e*).

#### 4.3 Light-Evenness

As mentioned in Section 2, the lighting in the LSC is an important factor affecting the quality of the scanned images. To measure the light evenness, we used a blank image (samples 3/5 in Fig. 2) as the reference and used the resulting scanned image of this blank envelope as the distorted image. Following image registration using the fiducial points, we computed the SSIM index value using only the luminance component and used this as our measure of light evenness. Although OQMA can be used for this process as well, the use of the same printing material for the reference and the LSC scanned images helps discount for the reflective behavior of the target. Because luminance changes are usually subtle, we discovered that using only the luminance term in SSIM did not provide a sufficient range of SSIM values to discriminate between cameras from different vendors. We addressed this issue by making

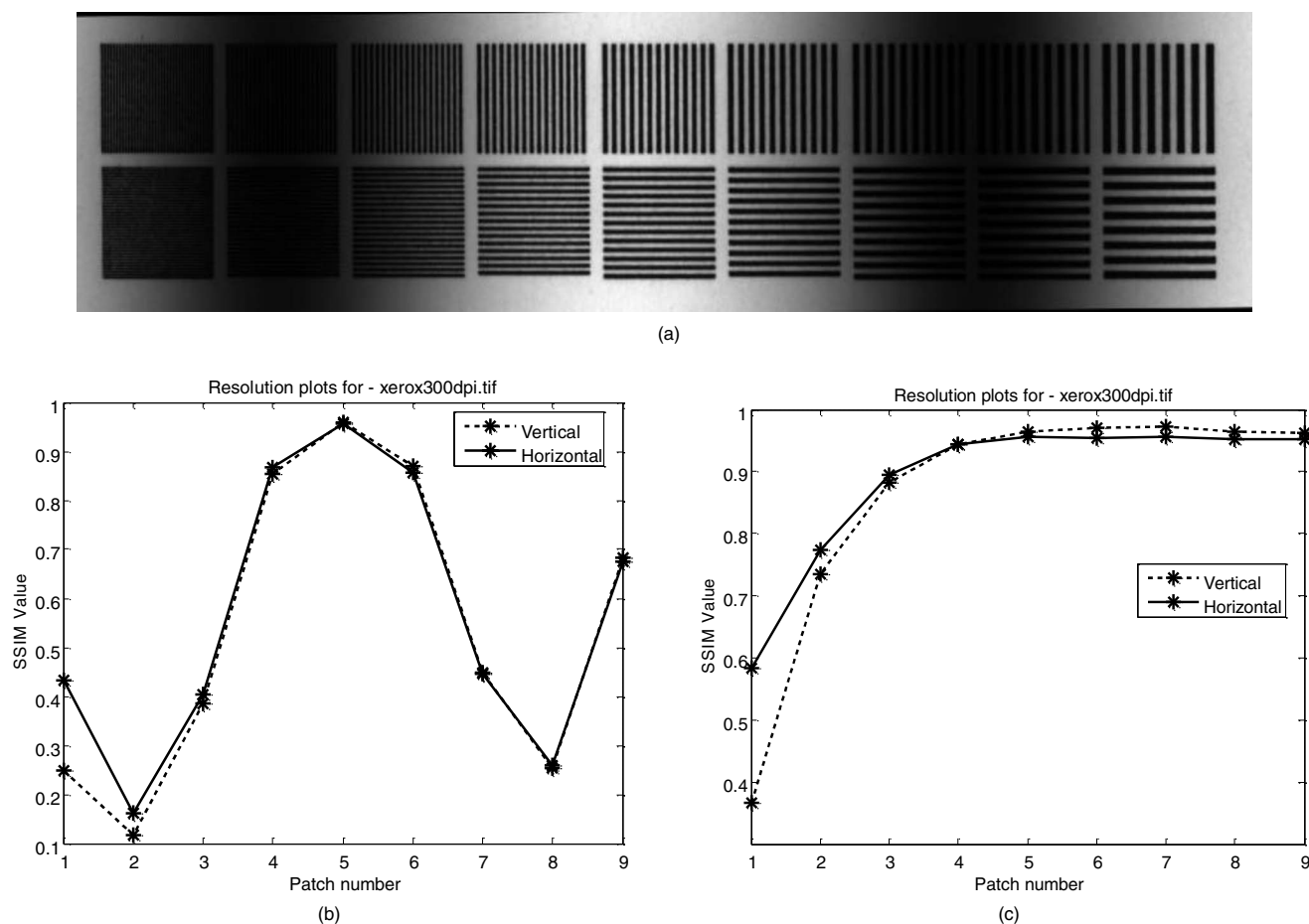


**Fig. 5** Effect of ambient illumination on OQCA measurements of resolution: (a) Simulation of a cosine illumination profile, (b) profile of the SSIM index values on the left is influenced by the ambient illumination, and (c) modified version of the SSIM discounts for the ambient illumination (when the luminance similarity term of the SSIM index is discarded).

the constant  $C_1$  in the definition of SSIM to be adaptive to the local mean luminance. In particular, we found that setting  $C_1 = -K\mu_I\mu_J$  with  $K$  ranging between 1.75 and 1.9 provided good discrimination between different cameras.

#### 4.4 Reflectance

One of the issues with mail scanning cameras is the fact that they have to scan letters with transparent windows. In the process of such a measurement, the system is bound to have reflections off the transparent material in the envelope and can potentially affect the quality of OCR. The luminance term of the SSIM Index between a reference image (which has no reflection) and an LSC scanned image is useful for measuring the distortion introduced by window reflections. The reference image in this case was obtained by scanning a document without a window, hence avoiding potential reflections in the reference image itself.

#### 4.5 Overall Image Fidelity

In addition to measuring SSIM for specific measurements as described here, we also computed the overall SSIM of the entire scanned image to provide a total quality score.

## 5 OQMA

OQCA cannot distinguish between certain distortions such as pin-cushion versus barrel distortion, positive versus negative skew, increased versus reduced brightness, etc. In such situations, it is convenient to simply measure the distortions directly without having to resort to pixelwise comparative imaging. Such techniques are categorized as OQMA in this paper. Because many OQMA techniques are common in the imaging community, we present only a brief description of the variables we used for evaluating the LSC.

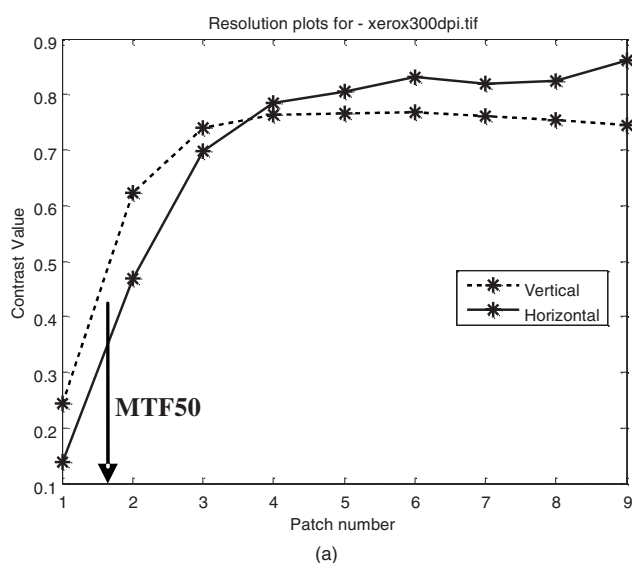
### 5.1 Effective Resolution

OQCA techniques to compute resolution are sensitive to the registration between the reference and the image generated by the LSC. It is therefore useful to have additional measurements of this important camera parameter that are independent of the reference image. One of the ways to measure effective resolution is based on research in measuring print quality.<sup>13-15</sup> Consider printing a periodic set of black bars on white paper. While printing very fine line patterns, the halftone patterns produced by the printer are large enough to overflow into the white space between two printed lines resulting in a reduced contrast image. This



**Fig. 6** Evaluating the quality of handwritten text: (a) 600-dpi scan of the handwritten test target, (b) image of the handwritten text as scanned by a LSC, and (c) SSIM map between the 600-dpi and LSC image. Bright regions in the map indicate good quality, while dark regions indicate poor quality. (d) Masked SSIM map. SSIM index is computed only around the text areas.

effect can be seen clearly in the right panel of Fig. 1. However, while printing patterns with lower lines per inch (lower spatial frequency), the spacing between the lines is much larger than the size of the halftone patterns and, therefore, the contrast between the dark lines and the white spacing between the lines does not decrease significantly. We used the same idea to quantify the effective resolution of the LSCs, where the decrease in contrast is a result of the low-pass modulation transfer function of the lens. The technique in Ref. 13 uses the difference in the gray scales between the bright and dark regions as a measure of contrast. However, this measure of contrast is sensitive to the average background luminance (see Fig. 5). By dividing the above measurement by the sum of the gray scales of the bright and dark regions, contrast can be made insensitive to background luminance. As a proof of principle, we scanned



the resolution pattern in Fig. 3 using a scanner at two settings of spatial resolution of 300 and 250 dpi. Figure 7 shows the resulting OQMA measurement of resolution for these scans. As can be seen, the contrast for the image scanned in at 300 dpi is higher than the image scanned at 250 dpi for the patches corresponding to the higher spatial frequencies (lower patch numbers). The patch number (lines per inch) at which resolution falls to 1/2 its value at low line density, known as MTF50 is often used to a system's resolving power. As shown in Fig. 7, the effective resolution measured using MTF50 is better for the image scanned using the scanner at 300 dpi. It is useful to note that the algorithm Ref. 13 uses only the minimum and maximum luminance gray-scale values to measure contrast. The SSIM-based OQCA measurement uses a more comprehensive feature by comparing the contrast and structural correlation and can therefore be expected to be a more robust/true measure of resolution. In addition to measuring the effective resolution, we also measured the native camera resolution (in pixels per inch) by detecting global fiducials and determining the number of pixels between them. Although native resolution does not reflect imaging quality directly,<sup>16</sup> cameras with higher pixels per inch are desirable because they can potentially capture finer variations.

## 5.2 Dynamic Range

Dynamic range of an imaging device is used to describe the difference (or ratio) between the minimum and maximum light intensities recorded or printed by the imaging device.<sup>17</sup> For our application, we computed the difference between the mean intensities of the black and white regions in pattern *b* of Fig. 2 as an indicator of dynamic range. The dynamic range of the printer used to print the test patterns should be higher than that of the LSC for the measurements to be meaningful.

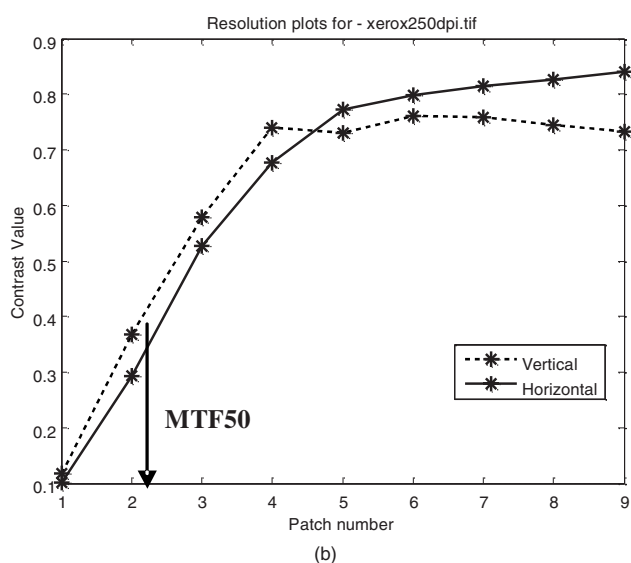


**Fig. 7** OQMA measurement of effective resolution: Contrast as a function of the patch number for a pattern printed at (a) 300 dpi and (b) 250 dpi. The dashed and solid lines correspond to the vertical and horizontal orientations of the bar patterns.

### 5.3 Noise

To measure the amount of noise in the LSC, we analyze the image of the gray-scale pattern  $b$  of Fig. 2. Each patch in this pattern was designed to have a uniform gray scale. However, the image produced by the LSC will not be uniform due to various sources of noise, such as randomness in the photons themselves, noise in the electronics of the camera, or in the postcapture quantization process. Thus, the variance of gray scales within a patch represents the energy of the noise introduced by the system. It is common practice to report the noise in a system using the SNR (in decibels), which is calculated as the ratio of dynamic range to the mean variance of each of the patch  $b$  of Fig. 2.<sup>17</sup> It is also useful to measure the noise in the lens-capped images (black images). It has been found that the noise in lens-capped images is best modeled using a Poisson distribution described as  $f(k) = e^{-\lambda} \lambda^k / k!$ .<sup>18</sup> The parameter  $\lambda$  is the mean and the variance of the distribution. The value of  $\lambda$  was computed by a maximum likelihood estimate and used as the measure of the dark noise in the system.

### 5.4 Skew

As mentioned earlier, the target used for scanning can undergo stretching, compressing, or angular distortion of a scanned image resulting from a lack of synchronization between the linear array and subject motion. Global rotations in the scanned image are measured by first detecting global fiducials located in each pattern and then measuring their angular deviation from the horizontal and vertical cardinal axis. Most test charts contain tick marks along the boundary of the test patterns (pattern  $g$  in Fig. 2). Local distortions such as shear are measured using these patterns. By design, the spacing between the tick marks were 0.125 in. We measured this intertick spacing in the scanned samples as used the mean deviation from 0.125 in. as an indicator of skew along either the horizontal or vertical axis.

### 5.5 Optical Distortion

It is well known that many lenses, especially those with a wide field of view, have optical distortions commonly known as pin-cushion or barrel distortion. We used the deviation of the distance between the points in pattern  $h$  in Fig. 2 from the expected distance between the points to quantify this distortion. An increase in the interdot spacing suggests barrel distortion, while a reduced interdot spacing suggests that the lens has pin-cushion distortions.

### 5.6 Optical Flare

Optical flare is the contrast reduction caused by surrounding stray light reflection on rapid dark to light image transitions. Our procedure of measuring flare involves the quantifying this decrease of contrast when a black image patch is imaged against a white background (sample  $c$  in Fig. 2). In particular, we measure the slope of the transition at the boundary of the dark and bright regions as an indicator of optical flare.

### 5.7 Light Evenness

Lighting in the LSC system is a major factor in the final image quality. The evenness of the light can obviously affect the quality of the scanned image. Light evenness was

measured by scanning a blank document (samples 3 and 5 in Fig. 2). The standard deviation of the resulting scan was used as an indication of light evenness. In addition, we also used pattern  $i$  in Fig. 2 to measure the light evenness.

### 5.8 Spectral Properties

Because the system has to scan ink of various colors, we quantified the RGB spectral reflectance by measuring the mean illumination of the patches (sample  $d$ ) in Fig. 2. The spectral range was computed as the difference between the mean values of the ends of the spectrum—the red and blue patches.

## 6 Discussion

In Sections 4 and 5, it was assumed that a pattern relevant to a certain measurement was easily accessible for processing. In practice, these patterns relevant have to be extracted from the images scanned by the LSCs. To automate this process, each target was designed with fiducial points that uniquely identified the location and alignment of various patterns. Given a scanned image, we first located these fiducial points using a National Instruments' template-matching algorithm.<sup>19</sup> Target-specific fiducials were then used to isolate a pattern of interest. Before analyzing a pattern using OQCA, the fiducial locations were used to align the LSC image to the corresponding reference image (scanned at 600 dpi using a flatbed scanner; see Section 4). Registration was performed using affine transformation and bilinear interpolation. The algorithm was implemented using National Instruments Vision Development Module and Microsoft Visual Studio.NET. Selecting between cameras from different vendors involved measuring all camera parameters and selecting the camera with the values closest to the values of the flatbed scanned. A statistically significant number of test scans ( $\sim 100$ ) were used to evaluate each vendor's camera performance. The code processed  $\sim 14,000$  images at a rate of  $\sim 2$  s per image. A table of measurements and their desired values are listed in Table 3.

OQCA can be used to measure several additional camera parameters that are currently measured exclusively using OQMA. The inherently ability of the modified SSIM (2) to separate luminance, contrast, and structural correlations allows for the following measurements. The luminance term in SSIM for the gray-scale gradient target (pattern  $b$  in Fig. 2) can be used to compute dynamic range; the contrast and luminance terms in SSIM for the gray-scale gradient targets can provide an indication of the SNR of the imaging system; the structure term in SSIM can be used to quantify optical distortions in the dot grid/array pattern; the structural term could also be used to measure the deviations in the tick marks along the image border to provide an indication of image skew.

Although OQCA measurements can potentially replace those made via OQMA, comparative imaging has some disadvantages that make OQMA a *sine qua non*. First, OQCA methods rely on accurate image registration between the reference and the distorted image. In its current form, the SSIM Index is sensitive to errors in image alignments. We addressed this problem by incorporating several global and pattern-specific fiducials that helped isolate and align the patterns with sufficient accuracy. Recent advances in shift-invariant, multiscale SSIM measurements<sup>20–22</sup> can also be

**Table 3** Definitions of each of the OQMA/OQCA measurements used to measure the performance of LSC cameras. The last column of this table indicates the desired value of each camera parameter.

OQMA	Units	Formula	Comments
Resolution (Horz)	ppi	Distance between global fiducial 1 and 2 (pixel)/ Actual distance between global fiducial 1 and 2 (in.)	Higher is better
Resolution (Vert)	ppi	Distance between global fiducial 2 and 4 (pixel)/ Actual distance between global fiducial 2 and 4 (in.)	Higher is better
Skew (Horz)	deg	Angle between global fiducial 1 and 2 (two top-most fiducials)	Smaller is better
Skew (Vert)	deg	Angle between global fiducial 2 and 4 (two right-most fiducials)	Smaller is better
Tick marks spacing (Horz)	in.	Mean distance between horizontal tick marks	Bogie=0.125 in.
Tick marks spacing (Vert)	in.	Mean distance between vertical tick marks	Bogie=0.125 in.
Distortion (Horz)	% error: 0–100	$[(\text{Mean distance between dots in horizontal (X-axis) direction—actual distance})/\text{Actual distance}] \cdot 100$	Barrel=positive Pincushion=negative
Distortion (Vert)	% error: 0–100	$[(\text{Mean distance between dots in vertical (Y-axis) direction—actual distance})/\text{Actual distance}] \cdot 100$	Barrel=positive Pincushion=negative
Flare (Horz)	Normalized: 0–1	Slope (between 10–90% level)/Range (black box mean—white box mean)	Best=1, worst=0
Flare (Vert)	Normalized: 0–1	Slope (between 10–90% level)/Range (black box mean—white box mean)	Best=1, worst=0
RGB spectral reflectance	Intensity level: 0–255	Mean intensity level for each color area	Higher is better
RGB spectral range	Intensity level: 0–255	Mean red—mean blue	Higher is better
Dynamic range	Intensity level: 0–255	Delta mean between black and white areas	Higher is better
SNR	dB: 0–48	$20 \log_{10} [\text{Mean Delta (dynamic range)}/\text{mean standard dev (all boxes)}]$	Higher is better
Light evenness		Standard deviation	Lower is better
Resolution	MTF50	Patch location at which resolution is at contrast 50	Lower is better
Effective resolution	PPI	Pixels per inch at which MTF reaches 50% of its value at low spatial frequencies	Higher is better
<b>OQCA</b>			
Overall SSIM	None	SSIM between reference and scanned image	Higher is better (max value is 1.0)
Text-based SSIM	None	Measures the fidelity of handwritten text	Higher is better (max value is 1.0)
SSIM window regions	None	Measures image fidelity in regions with transparent windows in test samples	Higher is better (max value is 1.0)

used to alleviate errors induced via misalignment. The second issue with comparative imaging is one of interpreting the SSIM values for a given camera parameter—an SSIM value of 0.7 does not provide an intuitive measure of that

particular parameter and is not necessarily twice as good as an image with a 0.35 SSIM index. In our application, this was not a problem because we were mainly interested in using these quality values to select between two or three

LSCs. However, if one desired to use OQCA to report the absolute value of a camera parameter, it would be necessary to calibrate the SSIM-based OQCA algorithms using OQMA measurements.

In conclusion, measuring the quality of a LSC is, in principle, similar to evaluating the quality of digital cameras, printers, or scanners. We showed that the low resolving power of LSCs obviates the need to use expensive test targets and allowed us to design application specific targets. Although OQMA reflects the current standard in measuring the quality of imaging devices, we demonstrated that novel OQCA techniques that can be used successfully in tandem to make other application-specific measurements.

## References

- ISO, "Photography—electronic still picture cameras—resolution measurements," ISO/TC WG18 (1998).
- P. D. Burns, "Slanted-edge MTF for digital camera and scanner analysis," in *PICS: Image Processing, Image Quality, Image Capture Systems Conference*, pp. 135–138, IS&T, Springfield, VA (2000).
- G. D. Boreman, *Modulation Transfer Function in Optical and ElectroOptical Systems*, SPIE Press, Bellingham, WA (1998).
- Z. Wang, A. C. Bovik, H. R. Sheikh, and E. P. Simoncelli, "Image quality assessment: from error visibility to structural similarity," *IEEE Trans. Image Process.* **13**(4), 600–612 (2004).
- Z. Wang and A. C. Bovik, *Modern Image Quality Assessment*, Morgan and Claypool Pub. Co., New York (2006).
- B. Girod, "What's wrong with mean-squared error?," *Digital Images and Human Vision*, MIT Press, Cambridge, MA, pp. 207–220 (1993).
- Z. Wang and A. C. Bovik, "Mean squared error: Love it or leave it? A new look at signal fidelity measures," *IEEE Signal Process. Mag.* **26**(1), 98–117 (2009).
- H. R. Sheikh, M. F. Sabir, and A. C. Bovik, "A statistical evaluation of recent full reference image quality assessment algorithms," *IEEE Trans. Image Process.* **15**(11), 3440–3451 (2006).
- M. v. Waldkirch, P. Lukowicz, and G. Troster, "Effect of light coherence on depth of focus in head-mounted retinal projection displays," *Opt. Eng.* **43**(7), 1552–1560 (2004).
- G. Piella and H. Heijmans, "A new quality metric for image fusion," in *Proc. Int. Conf. on Image Processing*, Vol. 2, pp. III-173–176, IEEE, Piscataway, NJ (2003).
- S. Kandadai, J. Hardin, and C. D. Creusere, "Audio quality assessment using the mean structural similarity measure," in *Proc. Int. Conf. on Acoustics, Speech and Signal Processing*, pp. 221–224, IEEE, Piscataway, NJ (2008).
- L. Snidaro and G. L. Foresti, "A multi-camera approach to sensor evaluation in video surveillance," in *Proc. Int. Conf. on Image Processing*, pp. I-1101–1104, IEEE, Piscataway, NJ (2005).
- D. Towner, N. Burningham, and E. Schneider, "An objective resolution metric for digital printers," in *PICS: Image Processing, Image Quality, Image Capture Systems Conference*, pp. 115–120, IS&T, Springfield, VA (2002).
- J. Hasegawa, T.-Y. Hwang, H.-C. Kim, D.-W. Kim, and M.-H. Choi, "Measurement-based objective metric for printer resolution," in *Image Quality and System Performance IV*, *Proc. SPIE* **6494**, 64940D (2007).
- W. Jang and J. P. Allebach, "Characterization of printer MTF," in *Image Quality and System Performance III*, *Proc. SPIE* **6059**, 60590D (2006).
- C.-L. Tisse, F. Guichard, and F. Cao, "Does resolution really increase image quality?," in *Digital Photography IV*, *Proc. SPIE* **6817**, 68170Q (2008).
- ISO, "Photography—Electronic still-picture imaging—Noise measurements," *ISO 15739:2003* (2003).
- C. Bonchelet, "Image noise models," *Handbook of Image & Video Processing*, A. C. Bovik, Ed., Academic Press, New York, pp. 325–335 (2000).
- "National Instruments Pattern Matching," (<http://zone.ni.com/devzone/cda/tut/p/id/3763>).
- Z. Wang and E. P. Simoncelli, "Translation Insensitive Image Similarity in Complex Wavelet Domain," in *Proc. Int. Conf. on Acoustics, Speech, and Signal Processing*, pp. 573–576, IEEE, Piscataway, NJ (2005).
- Z. Wang, E. P. Simoncelli, and A. C. Bovik, "Multiscale structural similarity for image quality assessment," in *Conf. Rec. 37th Asilomar Conference on Signals, Systems and Computers*, Vol. 2, pp. 1398–1402, IEEE, Piscataway, NJ (2003).
- M. P. Sampat, Z. Wang, S. Gupta, A. C. Bovik, and M. K. Markey, "Complex wavelet structural similarity: a new image similarity index," *IEEE Trans. Image Process.* **18**(11), 2385–2401 (2009).



**Umesh Rajashekar** received his BE in electronics and communication engineering from The Karnataka Regional Engineering College, India, in July 1998, and his MS from The University of Texas at Austin, in August 2000, joined the Laboratory for Image & Video Engineering (LIVE). He received his PhD in Fall 2005 and continued as a postdoctoral fellow at LIVE until August 2006, working on a project for Autim Inc. He was the assistant director of LIVE from 2001 to 2005, and is currently a postdoctoral fellow in the Laboratory for Computational Vision at the New York University.



**Tony Tuan Vu** received his BS in electrical and computer engineering from the University of Illinois at Urbana-Champaign, Urbana, in 1989, and MEng in electrical and computer engineering from the University of Illinois at Chicago, Chicago, in 2002. He is currently employed as a senior software engineer/manager at Autim/Innovative Imaging Inc., Chadds Ford, PA. His interests include image and video processing, machine vision, motion control, and Windows software development. He has also worked for Thomson/RCA, Cox Automations Systems, and Zenith Electronics. He holds one U.S. patent and one U.S. and international patent application pending.

**John E. Hooning:** Biography and photograph not available.



**Alan Conrad Bovik** is the Curry/Cullen Trust Endowed Chair Professor at The University of Texas at Austin, where he is the director of the Laboratory for Image and Video Engineering (LIVE). He is a faculty member in the Department of Electrical and Computer Engineering, the Department of Biomedical Engineering, and the Institute for Neuroscience. His research interests include image and video processing, computational vision, and visual perception. He has published more than 500 technical articles in these areas and holds two U.S. patents. He is the author of *The Handbook of Image and Video Processing* (Academic Press, 2005), *Modern Image Quality Assessment* (Morgan and Claypool, 2006), and two new books, *The Essential Guide to Image Processing* and *The Essential Guide to Video Processing* (Academic Press). He is a fellow of the IEEE, the Optical Society of America, and SPIE.